

# Advanced strategies for ion acceleration using high power lasers

A Macchi<sup>1,2</sup>, A Sgattoni<sup>1,3</sup>, S Sinigardi<sup>4</sup>, M Borghesi<sup>5,6</sup>, and M Passoni<sup>3</sup>

<sup>1</sup>Istituto Nazionale di Ottica, Consiglio Nazionale delle Ricerche (CNR/INO), U.O.S. “Adriano Gozzini”, Pisa, Italy

E-mail: andrea.macchi@ino.it

<sup>2</sup>Dipartimento di Fisica “Enrico Fermi”, Università di Pisa, Largo Bruno Pontecorvo 3, I-56127 Pisa, Italy

<sup>3</sup>Dipartimento di Energia, Politecnico di Milano, Via Ponzio 34/3, I-20133 Milan, Italy

<sup>4</sup>Dipartimento di Fisica e Astronomia and INFN, Università di Bologna, via Irnerio 46, 40126 Bologna, Italy

<sup>5</sup>Centre for Plasma Physics, The Queen’s University of Belfast, BT71NN Belfast, UK

<sup>6</sup>Institute of Physics of the ASCR, ELI-Beamlines Project, Na Slovance 2, 18221 Prague, Czech Republic

**Abstract.** A short overview of laser-plasma acceleration of ions is presented. The focus is on some recent experimental results and related theoretical work on advanced regimes. These latter include in particular target normal sheath acceleration using ultrashort low-energy pulses and structured targets, radiation pressure acceleration in both thick and ultrathin targets, and collisionless shock acceleration in moderate density plasmas. For each approach, open issues and the need and potential for further developments are briefly discussed.

PACS numbers: 52.38.-r 41.75.Jv 52.27.Ny

Submitted to: *Plasma Phys. Control. Fusion*

## 1. Introduction

Ion acceleration driven by superintense laser-plasma interaction with dense materials has been attracting an enormous interest in the last thirteen years because of the several foreseen applications such as fast ignition, medical hadrontherapy, nuclear and particle physics. Thanks to the continuous progress in high power laser technology and also in target manufacturing and engineering, several different acceleration mechanisms have been either demonstrated or proposed. Still, it is an open question to establish which mechanism is most promising for each application, as most of the requirements for ion

energy, conversion efficiency, spectral width, brilliance and suitability for high repetition rate operation have yet to be met.

In this paper we provide a partial update of our recent review of the field [1] (see also [2] for a complementary review) focusing on a selection of most recent results and emerging topics, and highlighting some contributions by our group. The emphasis is on basic acceleration mechanisms and general strategies to improve their performance.

## 2. Advances in Target Normal Sheath Acceleration of protons

Target Normal Sheath Acceleration (TNSA) is recognized as the basic mechanism of acceleration of protons from solid targets (typically in the  $0.1 - 10 \mu\text{m}$  thickness range) in most of the experiments reported so far, and has become the reference framework for source optimization. In TNSA, the protons are accelerated by the sheath field generated at the rear surface of the target by the energetic “fast” electrons accelerated at the front surface, where the laser-plasma interaction occurs. Thus, the enhancement of the maximum energy and conversion efficiency of protons is strictly related to the mechanisms of fast electron acceleration and transport through the target. Similarly, “engineering” of TNSA accelerating field by particular target shaping has been used for proton beam focusing and manipulation.

### 2.1. TNSA with ultrashort pulses

Several groups have investigated proton acceleration using laser systems with pulse durations of few tens of fs, typically delivering a total energy of a few Joules. Such laser systems have a compact size and potential for high repetition rate as required by most applications. The use of very tight focusing, producing laser spots with diameter of the order of one wavelength  $\lambda$ , combined with the ultrashort duration allows to reach intensities up to  $10^{21} \text{ W cm}^{-2}$ . The availability of pulses with very high contrast allows using very thin targets (from a few  $\mu\text{m}$  down to tens of nm) which in principle may yield higher densities and/or temperatures of fast electrons, and thus higher accelerating fields, due to the effects of energy confinement and electron recirculation.

Here we analyse a set of experiments with ultrashort pulses in an attempt to infer scaling and trends of the proton energy versus laser and target parameters. The data are taken from experiments performed in different laboratories i.e. HZDR Dresden (DRACO laser) [3, 4], LLNL Lund [5], GIST/APRI Gwangju (LiFSA) [6, 7], JAEA/KPSI Kyoto (JKAREN) [8] and CUOS Ann Arbor (HERCULES) [9]. This analysis is meant to update and be complementary to previously published surveys of data from different experiments and related inferred scalings, including comparison with theoretical models (see e.g. [2, 3, 10, 11, 12, 13, 14]).

Since in experiments the observed cut-off energy of protons  $E_{\text{co}}$  may be determined by the detection threshold, a proper comparison of different results may require to compare the full spectra or, at least, to take into account both  $E_{\text{co}}$  and the corresponding

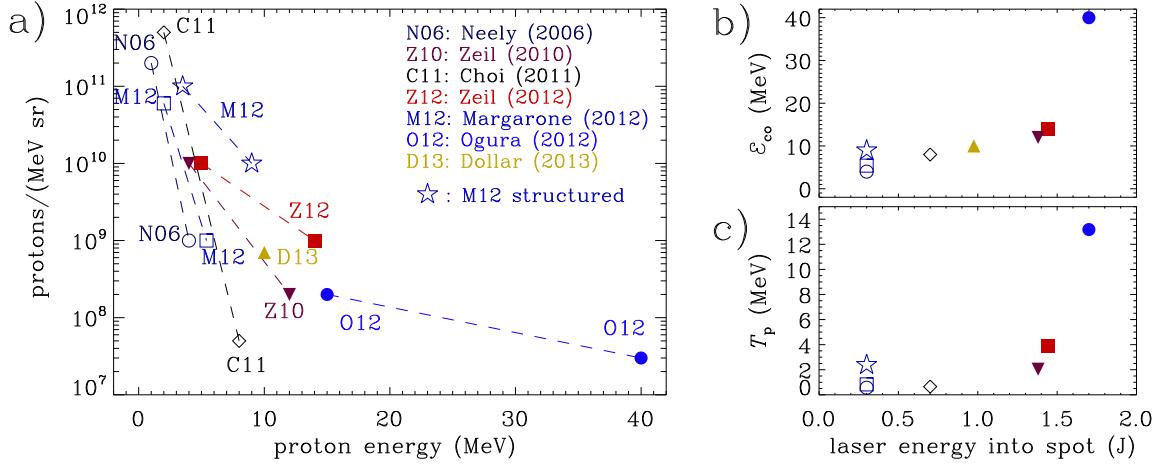


**Figure 1.** Proton energy from experiments using high contrast, sub-100 fs, sub-10 J laser pulses and thin solid targets. Data are from Refs.[5] (N06, empty circles), [3] (Z10, filled down-triangles), [6] (C11, diamonds), [4] (Z12, filled squares), [8] (O12, filled circles), [7] (M12, empty squares and stars) and [9] (D13, filled up-triangles). All target are planar foils of various thickness (in the  $0.05 - 4.0 \mu\text{m}$  range) except for data marked by stars which are for a structured target (thin foil covered by sub-micron size spheres). Data represented by empty and filled symbols are for intensities in the  $I = (1 - 5) \times 10^{19} \text{ W cm}^{-2}$  and  $I = (0.8 - 2) \times 10^{21} \text{ W cm}^{-2}$  ranges, respectively. The pulse durations are in the  $\tau = (25 - 40) \text{ fs}$  range. Frame a): spectral density of protons  $N_p(\mathcal{E})$  as a function of the proton energy  $\mathcal{E}$ . Dashed lines are simple exponential interpolations  $N_p(\mathcal{E}) = N_{p0} \exp(-\mathcal{E}/T_p)$  to observed complete spectra where available. Frame b): cut-off energy  $\mathcal{E}_{co}$  as a function of the laser pulse energy contained in the laser spot (defined as the area with diameter corresponding to the FWHM of the intensity profile). Frame c): the width parameter  $T_p$ , from exponential interpolations of the spectra in frame a), also as a function of the energy in the spot.

number density  $n_{co} = n_p(E_{co})$  with  $n_p$  the number of protons per energy and solid angle. Figure 1 a) summarizes available information by plotting  $n_p$  as a function of the proton energy  $E$  for the selected experiments. All reported spectra are well approximated by exponential functions  $n_p \sim \exp(-E/T_p)$ , “truncated” at the observed cut-off  $E_{co}$ .

In Fig.1 a) an increasing trend in both  $\mathcal{E}_{co}$  and  $T_p$  with the pulse energy is apparent. In detail,  $T_p$  has similar values for the low intensity data (empty symbols) while for the high intensity data (filled symbols)  $T_p$  increases with the pulse energy and is almost proportional to  $E_{co}$ . It is also noticeable that the data obtained for higher values of pulse intensity and energy correspond to lower values of the number of protons.

Fig.1 b) and c) show  $E_{co}$  and  $T_p$  as a function of the pulse energy in the laser spot, defined as the region corresponding to full-width-half-maximum (FWHM) of the intensity profile. This choice is made on the basis of available information on laser spot size and intensity distribution in Refs.[3, 4, 5, 6, 7, 8, 9] and allows accounting for different focusing optics and plasma mirror efficiencies as well as facilitating the comparison with theoretical models. The amount of energy in the laser spot is typically in the 20%-50% range of the total laser energy, and the values reported in Fig.1 b) and

c) fall in the  $< 2$  J range.‡

Fig.1 b) and c) show that  $E_{co}$  is roughly proportional to  $T_p$  with an increasing trend of both quantities with the laser pulse energy. The scaling with the laser intensity  $I$  appears instead to be much weaker than that with energy. The dependence on the target thickness does not show a clear trend, with the spread of observed values of  $E_{co}$  being much smaller than range of thicknesses ( $0.05 - 4.0 \mu\text{m}$ ). This latter observation is in qualitative agreement with parametric studies which show a relatively weak dependence on the target thickness in this regime [3, 4, 9, 15].

## 2.2. TNSA modelling

The above discussed experimental results may stimulate further advances in TNSA modelling. Since the first experiments there has been a demand for models yielding reasonably simple scaling laws, able to fit the observed dependencies on laser and target parameters. Ideally such theoretical effort should also reduce the need of additional empirical or “phenomenological” fitting parameters (such as, e.g., the maximum acceleration time) thus raising the predictive power of the models. Noticeably, several recent works have addressed the common problem of going beyond the assumption of a simple Maxwell-Boltzmann distribution for electrons, because of known problems with, e.g., the divergence of the accelerating potential at infinity (see e.g. Ref.[1], Sec.IIIC).

An extension of the static TNSA modelling for arbitrary electron distribution has been obtained by Schmitz [16]. Intriguingly, the use of an “universal” electron distribution proposed by Sherlock [17] on the basis of 1D simulations yields an upper limit of 66 MeV for the cut-off energy in the case of ultrashort pulse, when the ponderomotive scaling is used for the fast electron temperature, i.e.  $T_f = T_{\text{pond}}$  where

$$T_{\text{pond}} = m_e c^2 \left[ (1 + a_0^2/2)^{1/2} - 1 \right] , \quad (1)$$

and  $a_0 = 0.85(I\lambda^2/10^{18} \text{ W cm}^{-2}\mu\text{m}^2)^{1/2}$  is the dimensionless laser amplitude. A very close upper limit of 65 MeV has been also observed in 3D PIC simulations for simple flat targets and pulses with energy below 2 J [18]. Thus, going beyond such energy limit could require the exploitation of particular mechanisms of fast electron generation, providing a more favourable scaling than (1). The use of specially structured targets, to be discussed in the next section, is an effort in such direction.

Amongst static TNSA models, Passoni et al [19] have recently improved a previous model [12] by accounting for electron recirculation effects in thin targets. In this way a dependence of the cut-off value of the accelerating potential upon both target thickness and laser energy, which was previously inferred on an empirical basis, has been refined and motivated. A preliminary investigation (which will be reported elsewhere) with this

‡ Following our choice some quoted values of the “energy on target” have been corrected for the comparison. For example, in Refs.[3, 4] reporting experiments with the DRACO laser, it is reported that 80% of the laser energy is contained into a spot delimited approximately by the distance at which the intensity falls by  $e^{-2}$ . Assuming a Gaussian distribution, the energy in the smaller spot defined by the FWHM has been calculated and used in Fig.1 b) and c).

model of some of the experimental data reported in Fig.1 seems to confirm its predicting capabilities, highlighting at the same time novel open issues characterizing the TNSA regime when ultrashort and tightly focused laser pulses are used.

In the context of dynamic TNSA models, Kiefer et al [14] have revisited the problem of adiabatic plasma expansion for a steplike electron distribution. Deviations due to non-Maxwellian distributions are shown to be important and relevant to the interpretation of experiments. Kinetic effects in thin foil expansion have been also recently considered by Diaw and Mora [20].

For ultrashort pulses the assumption of quasi-equilibrium for electrons may become questionable. Zeil et al. [4] have experimentally investigated the “pre-thermal” stage of TNSA where the fast electrons in the sheath are out of equilibrium: the demonstration of proton beam steering by tilting the laser pulse wavefronts (resulting in a “target non-normal” acceleration) showed that the ultrashort laser pulse promptly affects the sheath parameters. Non-thermal acceleration of protons in the backward direction (towards the laser pulse) has been also investigated with extremely short (5 fs) pulses [21]. Here we sketch a very simple model of TNSA out of equilibrium. Assuming that electrons get to the rear surface with a momentum  $p_0 = m_e \gamma_0 v_0$  as short bunches separated in time by a laser period  $T_L = 2\pi/\omega_L$ , they turn back under the action of a uniform field that reverses the electron momentum to  $-p_0$  and thus gives a kick up to  $2p_0$  to protons at the surface. Since the number of kicks is  $\sim (\tau/T_L)$  with  $\tau$  the pulse duration, the total momentum gain is  $p_i = 2p_0(\tau/T_L)$  yielding an energy  $p_i^2/2m_i = (2p_0^2/m_i)(\tau/T_L)^2$ . Taking  $p_0 \simeq m_e c a_0$  we obtain a scaling  $\mathcal{E}_p \simeq 2m_e c^2 a_0^2 (\tau/T_L)^2 (m_e/m_p)$  similarly to Ref.[21]. If we rather model the fast electrons as a long bunch of density  $n_f$ , the field at the surface will initially grow in time as  $E_s = 4\pi e n_f v_0 t$ . As far as electron trajectories do not self-intersect, an electron emitted at the time  $t_0$  will return to the target at  $t_r = t_0 + 2p_0/E_s(t_0) = t_0 + 2\gamma_0/(\omega_{pf}^2 t_0)$  and the space-charge field will be largely cancelled at  $t_s = (2\gamma_0)^{1/2}/\omega_{pf}$  such that  $dt_r/dt_0 = 0$ . Protons will thus gain a momentum  $p_i \simeq e \int_0^{t_s} E_s(t) dt = m_e v_0 \gamma_0$  and an energy  $\mathcal{E}_p \simeq m_e v_0^2 \gamma_0^2 (m_e/2m_p) \sim m_e c^2 a_0^2 (m_e/m_p)$ . The second model should be more appropriate if  $T_L < t_r$ , i.e. for  $\omega_{pf}/\omega_L < (2\gamma_0)^{1/2}/2\pi$  which means that the fast electron density  $n_f$  should not largely exceed the critical density  $n_c = m_e \omega_L^2/(4\pi e^2)$ . We thus see that despite the fast scaling with  $a_0^2$  the proton energy gain is limited by the  $m_e/m_p$  factor.

For reasons of calculation feasibility almost all the analytical models of TNSA are one-dimensional, so that multi-dimensional effects may be addressed only by simulations, mostly performed using PIC codes. The increase of supercomputing power now allows large scale simulations to be performed up to three spatial dimensions (3D). This is particularly relevant for reliable quantitative predictions on TNSA because 3D simulations typically show proton energies lower by a factor of  $\gtrsim 2$  with respect to 2D simulations with the same parameters [18, 22]. At the same time, TNSA simulations remain very demanding because of issues such as large density variations in the sheath, steep gradients at the laser-plasma interface, and long duration of the acceleration stage.

### 2.3. TNSA in engineered targets

High-contrast pulses also allow to study the interaction with targets having nano- and micro-structured surfaces, since the structures may be not blown out by the prepulse. Thus, target engineering of various type has been investigated in order to optimize fast electron parameters (such as number, energy, and divergence) for more efficient TNSA.

Still for sub-10 J pulses, Margarone et al [7] have investigated targets covered by a monolayer of sub-micron spheres. These data are also shown in Fig.1 and the comparison shows an increase both in  $\mathcal{E}_{\text{co}}$  and in  $T_p$  with respect to flat targets at small angles of incidence. However, measurements with the same type of targets at the SLIC facility (CEA Saclay) have found TNSA enhancement to be almost absent at large angles of incidence [23].

At SLIC an increase in  $\mathcal{E}_{\text{co}}$  has been also observed in “grating” targets [24, 25] having a periodical surface modulation with sub-wavelength depth. For this experiment, Fig.2 a) shows  $\mathcal{E}_{\text{co}}$  as a function of the incidence angle for both grating and plane targets having a depth of  $\sim 20 \mu\text{m}$ . The laser pulse energy in the FWHM spot and the intensity were 0.3 J and  $2.5 \times 10^{19} \text{ W cm}^{-2}$ , respectively. The maximum enhancement is observed for the angle at which the resonant excitation of surface waves is expected. The achieved values of  $\mathcal{E}_{\text{co}}$  are somewhat limited by the large value of the target thickness, since the surface structuring of very thin foils is difficult. At the same time, the details of proton emission provide a very useful diagnostic for the laser absorption and electron acceleration mechanisms in the presence of microstructures.§

Use of “shaped” targets (having a structure size of the order of the laser spot, i.e. a few  $\mu\text{m}$ ) and high laser contrast allow also to achieve higher proton energies for pulse of relatively long duration (0.1 – 1 ps) and high energy ( $10^2 - 10^3$  J). Using specially designed microcone targets and the 80 J, 700 fs, high contrast pulse of the TRIDENT laser at LANL, Gaillard et al [27] were able to detect about  $10^7$  protons/MeV at a cut-off energy  $E_{\text{co}} = 67.5$  MeV, to be compared with  $E_{\text{co}} \simeq 50$  MeV in flat targets. The cut-off energy was higher than the long-lasting record of 58 MeV observed with  $> 400$  J pulses at the LLNL petawatt by Snavely et al [28]. However, it has to be noticed that in the spectrum measured in LLNL experiments  $\mathcal{E}_{\text{co}}$  corresponded to about  $10^9$  protons/MeV, a number for which the spectrum measured at TRIDENT for microcone targets yields about 40 MeV. Thus, the higher energy cut-off observed might be partly attributed to an increased sensitivity in the detector. Nevertheless, the cone target results also compare favourably with respect to those of Robson et al [29] which found protons up to 55 MeV at similar proton/MeV numbers using 400 J, 1 – 8 ps pulses from the VULCAN petawatt laser at RAL, and similar value of the target thickness.

The performance of the cone targets appears to be based on efficient electron

§ Using a particular form of cryogenic structured “snow” targets Zigler et al [26] have observed up to 21 MeV protons with a 2 J laser pulse at MBI Berlin. Both the number and emittance of such energetic protons appear to be lower than what is observed in TNSA experiments, and the acceleration is effective for low pulse contrast. Hence the acceleration mechanism is presumably quite different from TNSA.

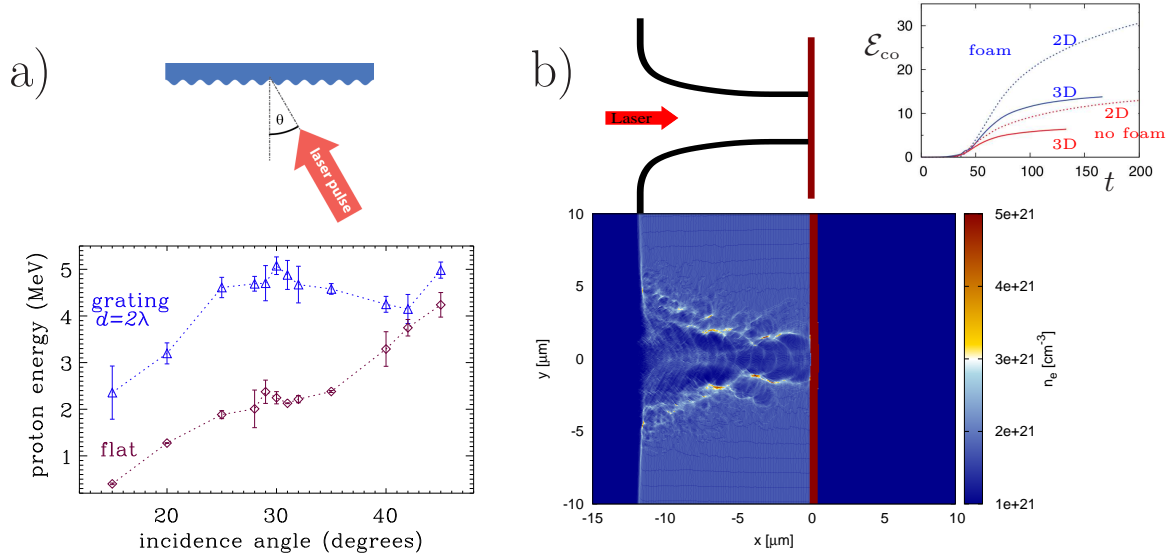


**Figure 2.** Examples of ion acceleration in “engineered” targets. Frame a): enhancement of cut-off proton energy in laser interaction with grating targets. The cut-off energy increases by a factor of  $\sim 2.5$  with respect to plane targets around the expected angle for resonant excitation of surface waves. Details can be found in Ref.[25]. Frame b): PIC simulation of channel boring in a low-density foam layer on the surface of a thin target. The cartoon shows the schematic of a cone target resembling the channel shape. The plot in the upper right frame reports the cut-off energy (in MeV) as a function of time (in fs) for 2D and 3D simulations, with and without the foam layer. The foam layer density and thickness are  $n_e = 2n_c = 3.4 \times 10^{21} \text{ W cm}^{-2}$  and  $d = 2\lambda = 1.6 \mu\text{m}$ . The laser pulse has peak amplitude  $a_0 = 10$  ( $I = 10^{20} \text{ W cm}^{-2}$ ), 25 fs duration and  $3 \mu\text{m}$  waist radius .

acceleration in cone geometry [30]. Indeed, some features of the acceleration mechanism such as coupling with the cone walls at local grazing incidence and existence of an optimal cone length are also apparent in simulations of channel drilling in a near-critical density plasma [22]. In a thin target covered with a near-critical layer, efficient electron acceleration may yield electron temperatures up to  $T_f \simeq 3T_{\text{pond}}$  and up to a three-fold increase in  $E_{co}$  with respect to targets without foam layers: see the simulation results shown in Fig.2 b) where the effect of 3D geometry versus 2D is also shown. Simulations of this scheme have been performed so far for ultrashort, low-energy pulses because of computational limitations. Also experimentally the scheme has been tested in the short-pulse regime and with foam thicknesses suitable to imply a gain at low intensity conditions [31, 32]. Further investigations with longer pulses are needed to compare with cone targets.

#### 2.4. Proton focusing and spectral manipulation

Suitably shaped targets have been also used since the first experiments to focus the proton beam, without the need of an external steering system and allowing the focusing of large number of protons as it would be required by fast ignition and high energy

density physics applications. Recently, progress on this side has been obtained by Bartal et al [33] on TRIDENT using cone targets similar to those designed for fast ignition research. Focusing by concave targets has been investigated also at LULI [34] revealing an issue of proton beam filamentation and emittance degradation.

Another possibility of present interest is based on the use of the strong quasistatic magnetic fields generated during the laser-plasma interaction and related to the process of sheath formation and evolution itself. Early analysis of experiments on ultrathin foils traced back spectral modulations in the low-energy part of the proton spectrum to the effect of magnetic fields  $>10$  MG generated at the rear surface within tens of fs [35]. Measurements based on the proton probing technique [36] gave both evidence of the generation of fields of several tens of MG by the “fountain effect” of fast electrons [37] and of their capability to either focus or defocus multi-MeV protons. Very recent experiments on the TITAN laser at LLNL have tested this concept [38].

The engineering of target geometry and composition has been also investigated with the aim to manipulate the TNSA spectrum and obtain suitably monoenergetic distributions reducing the need of external filtering devices (see e.g. sec.III.E.2 in Ref.[1]). However, recently there seems to have been little progress on this side. For instance a seemingly promising approach based on targets with nanolayers deposited on their rear side [39, 40] has not been further developed. These issues, as well as the uncertainties in reaching via TNSA-based schemes the high energies  $> 100$  MeV/nucleon required by some applications, motivate the search for alternate mechanisms which we describe in the next sections.

### 3. Towards Radiation Pressure Acceleration

#### 3.1. RPA in thick targets: hole boring

The radiation pressure of an intense laser pulse pushes the plasma surface inwards, creating a bow-shaped deformation. For thick targets, such that the deformation front does not reach the rear side of the target during the pulse, this regime has been commonly named as “hole boring” (HB). Assuming a uniform density, cold plasma target with mass density  $\rho = Am_p n_i = (A/Z)m_p n_e$ , the fastest ions have an energy per nucleon (see sec.IV.A.1 of Ref.[1] and references therein)

$$\mathcal{E}_{\text{HB}} = 2m_p c^2 \frac{\Pi}{1 + 2\Pi^{1/2}}, \quad \Pi = \frac{I}{\rho c^3} = \frac{Z m_e n_c}{A m_p n_e} a_0^2. \quad (2)$$

corresponding to twice the velocity of the receding surface  $v_{\text{HB}} = c\Pi^{1/2}/(1 + \Pi^{1/2})$ . Recently a theory of HB-RPA including effects of temperature, pulse envelope and density inhomogeneity has been presented by Levy et al [41] who also discuss possible relevance of HB experiments to astrophysical scenarios, such as Poynting flux-dominated outflows.

Simulations of HB-RPA show that the fast ions may have a narrow energy spread and thus lead to a non-thermal, peaked ion energy spectrum particularly for a circularly



polarized pulse at normal incidence since fast electron generation and, consequently, TNSA are strongly suppressed. Protons with energy  $\simeq 1$  MeV and  $\simeq 10\%$  energy spread were observed in an experiment at Brookhaven National Laboratory (US) [42] where a circularly polarized  $\text{CO}_2$  pulse of amplitude  $a_0 = 0.5$  and a gas H jet target were used allowing values of  $n_e/n_c \gtrsim 1$ . The potential advantages of this experimental scheme are the reduction of the electron density to increase  $\mathcal{E}_{\text{HB}}$ , the pure proton plasma and the suitability for high repetition rate.

The scaling with density makes the transition to HB-RPA hard to observe in solid targets where  $n_e \gtrsim 10^2 n_c$ . However, either the presence of a significant preplasma or the use of advanced targets at low density (liquid hydrogen jets would be particularly suitable) may allow to work with  $n_e/n_c \gtrsim 1$  also with optical lasers. The approach might be of interest especially for next-generation short-pulse lasers aiming at very large values of  $a_0$  with modest pulse energy and possibly allowing high repetition rate operation. Related simulation studies and suggestions for experiments have been reported in Refs.[43, 44, 45].

### 3.2. RPA in thin targets: light sail

For thin targets of thickness  $\ell \ll v_{\text{HB}}\tau$ , RPA enters into the “light sail” (LS) mode in which the whole target is accelerated. For LS, the scaling is now with the pulse fluence  $I\tau$  (total energy per unit surface) divided by the areal density of the target (see sec.IV.A.2 of Ref.[1] and references therein):

$$\mathcal{E}_{\text{LS}} = m_p c^2 \frac{(\Omega\tau)^2}{2(\Omega\tau + 1)}, \quad \Omega = \frac{2I}{\rho\ell c^2} = T_L^{-1} \frac{Z}{A} \frac{m_e}{m_p} \frac{a_0^2}{\zeta}, \quad \zeta = \pi \frac{n_e}{n_c} \frac{\ell}{\lambda}. \quad (3)$$

The LS operation is limited by the onset of relativistic transparency when  $a_0 > \zeta$ , thus the “optimal” matching of the areal density with the pulse amplitude occurs for  $a_0 = \zeta$ .|| This condition is presently accessible thanks to manufacturing techniques for foils as thin as a few nm, for which typically  $\zeta \lesssim 10$ . Of course ultrahigh contrast is necessary for this type of experiment. Posing  $a_0 = \zeta$  and  $Z/A = 1/2$  in Eq.(3) and assuming non-relativistic ions ( $\Omega\tau \ll 1$ ), we may write a simplified scaling law for LS-RPA using optimal thickness targets:

$$\mathcal{E}_{\text{LS}}^{(\text{opt})} = \frac{m_e^2 c^2}{8m_p} a_0^2 \left( \frac{\tau}{T_L} \right)^2 \simeq 2.3 \text{ MeV} \times \frac{I\tau^2}{10^{-6} \text{ J s cm}^{-2}} = 2.3 \text{ MeV} I_{20} \tau_{100}^2, \quad (4)$$

where  $I_{20}$  and  $\tau_{100}$  are the intensity and pulse duration in units of  $10^{20} \text{ W cm}^{-2}$  and 100 fs, respectively. The more favourable scaling with pulse duration than with intensity is due to the latter being limited by the transparency threshold. Eq.(4) shows that energies  $> 100$  MeV per nucleon are within reach of present-day petawatt systems.

|| Strictly speaking this condition is derived on the basis of a simple model of delta-like foil plasmas and has been verified by simulations using circularly polarized, ultrashort pulses (see e.g. Ref.[46]). In more general cases the “optimal” thickness value determined by transparency effects may have a more complex dependence on the laser pulse parameters (see e.g. Refs.[47, 48, 49]).

Several recent experiments have investigated the interaction with ultrathin foils obtaining indications of the onset of LS-RPA. Using the VULCAN petawatt pulse ( $\sim 800$  fs,  $I = 0.5 - 3 \times 10^{20}$  W cm $^{-2}$ ) Kar et al observed spectral peaks for both protons and heavier (e.g. carbon) ions, with energies up to 10 MeV/nucleon, and inferred from data a scaling of the peak energy as  $(\Omega\tau)^2$  in accordance with Eq.(3) for  $\Omega\tau \ll 1$ . Similar results have been obtained by Aurand et al [50] using the much shorter pulse (27 fs,  $I = 0.2 - 6 \times 10^{19}$  W cm $^{-2}$ ) of the JETI laser at Jena. Common to both experiments was a weak dependence upon the laser polarization and a separation in the spectrum between proton and carbon peaks. Thus, the acceleration occurs in the presence of fast electrons, and the peak separation might be due to additional TNSA-like effect giving an extra boost preferentially to the lighter protons. Similar spectra were also obtained by Steinke et al [51] at MBI Berlin using circular polarization only. This suggests that side effects such as the tight focusing of the laser pulse ( $f/2.5$  for Ref.[51]) cause significant heating also for circular polarization, because of both the non-negligible longitudinal electric field components and the target deformation which leads to locally oblique incidence. For even tighter focusing ( $f/1$ ), using the HERCULES laser at  $I = 2 \times 10^{21}$  W cm $^{-2}$  Dollar et al [52] found that finite spot size effects almost cancel out the differences between linear and circular polarization and are unfavourable for RPA.

Recent results by Kim et al [53] obtained with the 30 fs PULSER laser at GIST using ultrathin targets, linear polarization and  $f/4$  focusing with an intensity range  $I = 0.5 - 3.3 \times 10^{20}$  W cm $^{-2}$  show a more complex scenario. Non-thermal, peaked spectra are observed for C ions while the proton spectrum is broad, modulated and extends up to a cut-off energy  $\mathcal{E}_{co} = 45$  MeV for the thinnest target (10 nm). The number of accelerated protons appears to be higher by an order of magnitude than those observed for thicker targets by Ogura et al [8] at a similar cut-off energy. In addition, varying the intensity showed a transition from a  $\mathcal{E}_{co} \propto I^{1/2}$  to  $\mathcal{E}_{co} \propto I$  at an intermediate intensity (with the peak energy of carbon spectra showing a similar trend). This trend (also apparent in the peak energy of C) is similar to that observed by Esirkepov et al in multi-parametric simulations [49] and attributed to the progressively dominant role of RPA. For the thinnest target values, however, one would also expect a strong effect of relativistic transparency, which might account for the broad proton spectra. Comparison with PIC simulations also suggests that the modulations in the energy spectrum are due to a transverse instability of the foil target, similarly to previous measurements on VULCAN [54].

As an overall comment on the above mentioned experiments, the importance of RPA effects at the highest intensities (or in more generally suitable conditions) is apparent and the evidence of the “fast” quadratic scaling with fluence is promising. Still, a long way towards optimization remains. In particular, the non-thermal spectra observed for thin foils are relatively broad, in contrast to the simple picture of LS-RPA as a thin plasma bunch moving at a coherent velocity, which would correspond to a perfectly monoenergetic spectrum. The need for wide laser spots to prevent target bending and

excessive heating would imply large amounts of laser energy. Many observed features need to be fully understood, especially the RPA dynamics with multiple species. Such effects could be also exploited to stabilize the acceleration, and more in general target engineering might also be pursued to tailor the spectrum (see several references in Ref.[1], sec.IV.A.2).

### 3.3. RPA as a route towards relativistic ions

In LS-RPA the conversion efficiency  $\eta = 2\beta_{\text{LS}}/(1 + \beta_{\text{LS}})$  reaches unity when the sail velocity  $\beta_{\text{LS}} \rightarrow 1$ . However, the scaling with the pulse fluence is less favourable in this regime. Assuming again  $a_0 \simeq \zeta$  at the optimal condition we obtain  $\mathcal{E}_{\text{LS}}^{(\text{opt})} = (m_e c^2 a_0 / 2) (\tau / T_L)$ . Based on this estimate the laser fluence required to reach  $\mathcal{E}_{\text{LS}} = m_p c^2$  is  $1.5 \times 10^8 \text{ J cm}^2$ . The corresponding energy would depend strongly on the possible requirement of a sufficiently wide spot to minimize effects of target deformation: as an example, taking a  $10 \text{ }\mu\text{m}$  diameter would require 120 J energy. The slow rate of energy gain in the laboratory frame as  $\mathcal{E}_{\text{LS}} \sim (\Omega t)^{1/3}$  also represents a possible issue since the acceleration distance might be large enough that pulse diffraction must be taken into account.

While these issues are certainly challenging, theory and simulation have identified possible regimes of high gain LS-RPA in the relativistic ion regime. Using 2D simulations and analytical modelling Bulanov et al [55] have shown how the target rarefaction might dynamically reduce the areal density on the axis. This allows a faster energy gain  $\mathcal{E}_{\text{LS}} \sim (\Omega t)^{3/5}$  at the expense of a lower number of accelerated ions, provided that a transition to transparency (partly prevented by the decrease of laser pulse frequency in the target frame) does not occur. Tamburini et al [56] have further investigated this regime with fully 3D simulations, finding that the energy maximum observed in 3D simulations is *higher* than in 2D, since the effects of rarefaction are stronger. Exploiting the computing power of the FERMI supercomputer at CINECA (Bologna, Italy) the simulations of Ref.[56] have been extended to longer times. Fig.3 a) shows the maximum energy as a function of time, which is well fitted by the  $(\Omega t)^{3/5}$  scaling up to a time of  $t = 30T_L$ . At later times the growth becomes slower, presumably because of the onset of strong transmission of the pulse through the target. The energy of  $\simeq 2.6 \text{ GeV}$  at  $t = 60T_L$  is more than six times the prediction of the 1D formula (3) for  $\mathcal{E}_{\text{LS}}$ . These results show that multi.GeV energies might be reached with pulse energies of the order of 1 kJ, combined with pulse durations and focusing suitable to approach the  $10^{23} \text{ cm}^{-3}$  intensity level (in the case of Fig.3 a waist radius of  $6\lambda$  and a pulse duration of 24 fs were used). The spatial distribution in Fig.3 b) shows that the most energetic ions are collimated into a narrow cone.

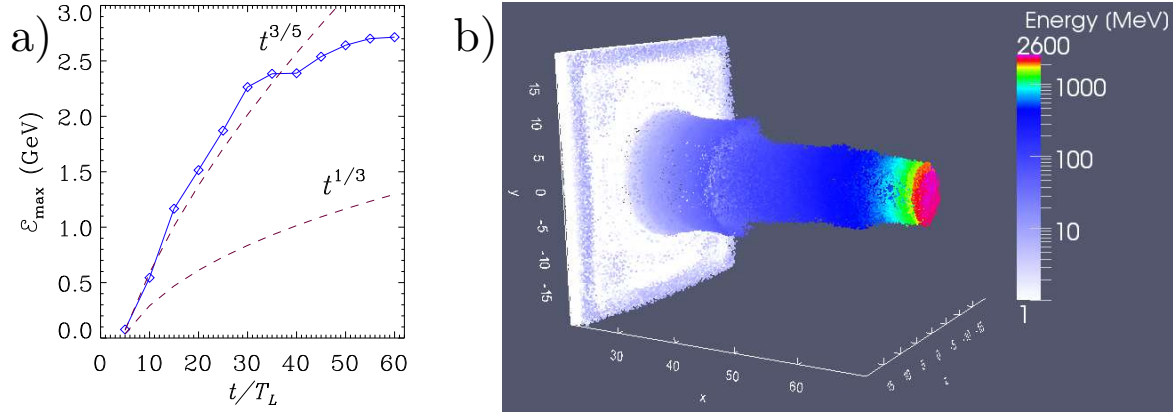


**Figure 3.** 3D simulations of LS-RPA. Frame a): maximum ion energy versus time (in laser cycles). Frame b): distribution in space and energy of ions directed into a cone with  $10^\circ$  full aperture. The target has an initial thickness  $\ell = \lambda$  and density  $n_e = 64n_c$  ( $= 1.1 \times 10^{23} \text{ cm}^{-3}$  for  $\lambda = 0.8 \mu\text{m}$ ) corresponding to  $\zeta \simeq 200$ . The laser pulse has  $9T_L$  (24 fs) FWHM duration (“ $\sin^2$ ” envelope),  $a_0 = 198$  peak amplitude ( $I = 8.5 \times 10^{22} \text{ W cm}^{-2}$ ),  $6\lambda$  ( $4.8 \mu\text{m}$ ) waist radius, and circular polarization.

#### 4. Acceleration in the relativistic transparency regime

While the onset of relativistic transparency in a thin target stops the LS-RPA stage, it opens up a regime of volumetric interaction with the near-critical density plasma which may lead to high ion energy. In particular, proton cut-off energies exceeding 100 MeV have been communicated [57]. Several experiments in the transparent regime have been performed with TRIDENT at LANL (see e.g. Ref.[58] for a review of results oriented to fast ignition ICF research). Most of the observation are explained in the context of the Break-Out Afterburner (BOA) model which is actually a relatively complex mechanism, involving strong instability stages which lead to strong heating of electrons and coupling to ions. While scalings with laser and target parameters have probably to be fully characterized yet, BOA has shown promising results for what concerns cut-off energies and number of ions. A recent work [59] shows in particular an efficient bulk acceleration of C ions, producing up to  $5 \times 10^{11}$  particles with an high efficiency of 6%.

A typical signature of the onset of the transparent regime is that the highest ion numbers and energies are not detected along the laser axis at some angle (e.g.  $10^\circ$  for Ref.[59]). This effect is also observed in 3D simulations analogous to that shown in Fig.3 but for linear polarization. In such a case the transmission of the laser pulse is stronger than for circular polarization and the maximum energy is lower.

#### 5. Collisionless Shock Acceleration

An experiment with a similar set-up to Ref.[42], i.e. using a  $\text{CO}_2$  laser and a hydrogen jet target was also performed with the NEPTUNE laser at UCLA (US) [60]. In this case the laser polarization was linear and the intensity of was four times higher than in Ref.[42].

Very narrow peaks in the proton spectrum were observed up to 22 MeV with  $\simeq 10^7$  protons  $\text{MeV}^{-1}\text{sr}^{-1}$  in the peak, in striking contrast with  $> 10^{12}$  protons  $\text{MeV}^{-1}\text{sr}^{-1}$  at  $\simeq 1$  MeV for Ref.[42] which gives evidence of a different acceleration mechanism.

The UCLA experiment was interpreted on the basis on the Collisionless Shock Acceleration (CSA) model. The fast heating of electrons and density steepening by the laser pulse drive collisionless shock waves at the velocity  $v_s = Mc_s$  (where the sound velocity  $c_s = (ZT_e/Am_p)^{1/2}$  for a non-relativistic plasma and electrons in Boltzmann equilibrium, and  $M > 1$  is the Mach number). These shocks are associated to ions reflected by the shock front. As far as  $v_s$  is constant the reflected ions form a monoenergetic beam at the velocity  $2v_s$ . If the shock is sustained by fast electrons ( $T_e = T_f$ ) high values of  $v_s$  and of ion energies  $m_p(2v_s)^2/2 = 2m_pv_s^2$  may be reached. Much theoretical and simulation work has been performed to unfold the details of the acceleration process and in particular to tailor the plasma density profile obtaining a suitably smooth plasma gradient, with the additional aim to suppress TNSA in favour of CSA (see [61] and references therein).

Scaling CSA beyond 100 MeV/nucleon will require either the development of  $\text{CO}_2$  lasers with higher energy or a suitable set-up with optical lasers, using target at densities around  $n_c \simeq 10^{21} \text{ cm}^{-3}$  which is higher than what is commonly achieved with gas jets. Recent experiments were performed at LULI using exploding foil plasmas (pre-heated by long pulses) which turn underdense at the time of the interaction with a short intense pulse [62]. With this method, broad proton spectra up to a cut-off energy of 7.1 MeV with  $\simeq 10^9$  protons  $\text{MeV}^{-1}\text{sr}^{-1}$  have been obtained with a 8 J, 400 fs,  $5 \times 10^{18} \text{ W cm}^{-2}$  laser pulse [63].

A possibly limiting factor in CSA is that high efficiency may be not compatible with keeping a monoenergetic spectrum. This is because the energy gained by the accelerated ions is at expense of the shock wave energy, so that the shock velocity decreases. In turn, the velocity of the reflected ions decreases as well, causing a progressive chirp of the spectrum towards low energies [64]. To illustrate the basics of the effect and its dependence on the initial velocity distribution of the background ions, we show in Fig.4 the results of two 1D PIC simulations with identical parameters but different initial temperature  $T_i$ . For higher  $T_i$ , a larger number of ions is reflected from the shock, causing a stronger loading of the shock front which velocity decreases. As a consequence the peak in the spectrum broadens in time. This effect may explain why the monoenergetic spectra of Ref.[60] correspond to quite low number of protons. This is also an issue for PIC simulations because a very low energy tail needs to be resolved, requiring very high numbers of computational particles.

## 6. Conclusions

There has been considerable recent progress in laser-driven ion acceleration. In the last two years the observed energy cut-offs have increased with short pulse, low energy laser systems reaching several tens on MeV, close to or even exceeding what was obtained

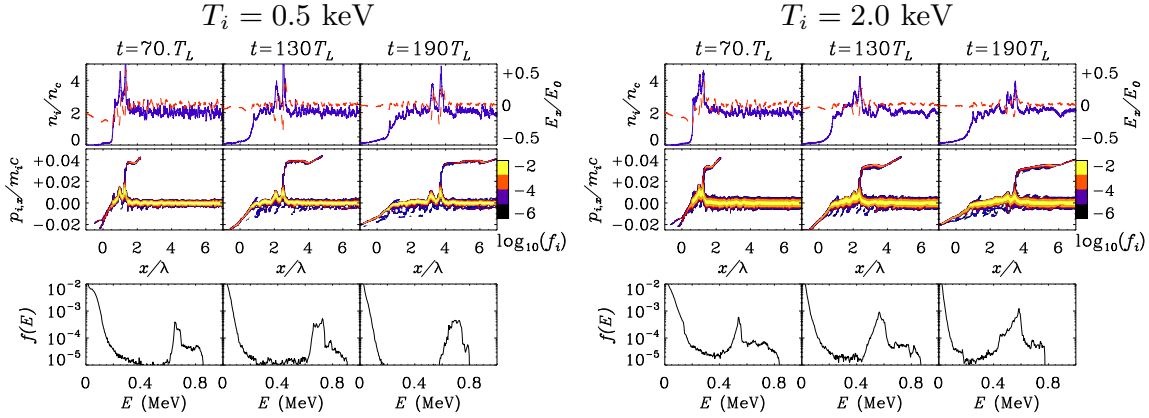


**Figure 4.** One-dimensional PIC simulation of shock acceleration. Results are shown for two runs with identical parameters but the initial ion temperature  $T_i$  (0.5 and 2 keV, respectively). For both simulations snapshots at three different times (in units of the laser period  $T_L$ ) are shown. The laser pulse impinges from the left and reaches at  $t = 0$  the plasma boundary at  $x = 0$ . The top row shows the profiles of ion density  $n_i$  and electric field  $E_x$ . The middle row shows the  $f_i(x, p_x)$  projection of the ion phase space distribution. The bottom row shows the ion energy spectrum. For higher  $T_i$  the shock velocity decreases and the spectrum progressively broadens towards lower energies. The laser and plasma parameters are  $a_0 = 1$ ,  $\tau = 55T_L$ ,  $n_e = 2n_c$ . The density and the electric field are normalized to  $n_c$  and  $m_e\omega c/e$ , respectively.

with large petawatt systems. Progress have been also obtained on the side of conversion efficiency, total number of particles, and energy spread. It might be argued that on each side the most promising results have been obtained in different experiments with no acceleration mechanism at present seeming able to combine all desirable qualities. However, there appears to be room for further optimization, with each mechanism being ultimately most suitable for a specific application.

Ultrahigh pulse contrast has played a crucial role in experiments with solid targets, allowing for instance the use of ultrathin foils, and probably has allowed more controlled conditions and more reproducible observations. Promising results have been also achieved by the use of structured targets, with ion acceleration also providing an insight on the peculiar interaction physics. The development of innovative targetry has a crucial importance also for the perspective of high-repetition rate operation.

The further development of high-power laser systems will allow soon to extend the present investigations to unexplored regimes. Relevant laser development may not only involve optical systems with femtosecond pulses but also CO<sub>2</sub> infrared lasers which are of potential interest for radiation pressure and shock acceleration in gas targets.

Significant advances have also been made on the side of modelling of experiments and understanding of relevant physics. Still, however, several open questions remain and in several cases theoretical scalings with laser and target parameters are still uncertain. Further progress on this side is highly desirable, especially in order to provide reliable predictions on experiments with next-generation laser systems. In particular

there is a strong need, common to different acceleration mechanisms, for massively parallel simulations able to perform more realistic investigations, in a three-dimensional geometry and over large scales of space and time.

## Acknowledgments

A.M. thanks J. Fuchs (LULI, École Polytechnique, France), K. Zeil (HZDR, Germany), E. d’Humières (CELIA, France), D. Margarone (ELI-Beamlines, Czech Republic) and Chul Min Kim (GIST, Korea) for providing additional information and comments on published and unpublished results. The grating targets data of Fig.2 have been obtained in an experiment at the SLIC facility (CEA Saclay, France) funded from LASERLAB-EUROPE (grant agreement no. 284464, EU’s 7FP, proposal n.SLIC001693) and were analysed by T. Ceccotti and V. Floquet. The contribution of P. Londrillo to ALaDyn code development and simulations is gratefully acknowledged. Access to FERMI supercomputer at CINECA was awarded by PRACE via the project “LSAIL”. Support from EPSRC, grant EP/E035728/1 (LIBRA consortium) and from the Italian Ministry of University and Research via the FIR project “SULDIS” is acknowledged.

## References

- [1] Macchi A, Borghesi M, and Passoni M. Ion acceleration by superintense laser-plasma interaction. *Rev. Mod. Phys.*, 85:751–793, 2013.
- [2] Daido H, Nishiuchi M, and Pirozhkov A S. Review of laser-driven ion sources and their applications. *Rep. Prog. Phys.*, 75:056401, 2012.
- [3] Zeil K et al. The scaling of proton energies in ultrashort pulse laser plasma acceleration. *New J. Phys.*, 12:045015, 2010.
- [4] Zeil K et al. Direct observation of prompt pre-thermal laser ion sheath acceleration. *Nature Comm.*, 3, 2012.
- [5] Neely D et al. Enhanced proton beams from ultrathin targets driven by high contrast laser pulses. *Appl. Phys. Lett.*, 89:021502, 2006.
- [6] Choi I W et al. Simultaneous generation of ions and high-order harmonics from thin conjugated polymer foil irradiated with ultrahigh contrast laser. *Appl. Phys. Lett.*, 99:181501, 2011.
- [7] Margarone D et al. Laser-driven proton acceleration enhancement by nanostructured foils. *Phys. Rev. Lett.*, 109:234801, 2012.
- [8] Ogura K et al. Proton acceleration to 40 MeV using a high intensity, high contrast optical parametric chirped-pulse amplification/ti:sapphire hybrid laser system. *Opt. Lett.*, 37:2868–2870, 2012.
- [9] Dollar F et al. High contrast ion acceleration at intensities exceeding  $10^{21}$  W cm<sup>-2</sup>. *Phys. Plasmas*, 20:056703, 2013.
- [10] Fuchs J et al. Laser-driven proton scaling laws and new paths towards energy increase. *Nature Phys.*, 2:48, 2006.
- [11] Borghesi M et al. Laser-driven proton acceleration: source optimization and radiographic applications. *Plasma Phys. Contr. Fusion*, 50:124040, 2008.
- [12] Passoni M, Bertagna L, and Zani A. Target normal sheath acceleration: theory, comparison with experiments and future perspectives. *New J. Phys.*, 12:045012, 2010.
- [13] Perego C, Zani A, Batani D, and Passoni M. Extensive comparison among target normal sheath acceleration theoretical models. *Nucl. Inst. Meth. Phys. Res. A*, 653:89 – 93, 2011.

- [14] Kiefer T, Schlegel T, and Kaluza M C. Plasma expansion into vacuum assuming a steplike electron energy distribution. *Phys. Rev. E*, 87:043110, 2013.
- [15] Prasad R et al. Fast ion acceleration from thin foils irradiated by ultra-high intensity, ultra-high contrast laser pulses. *Appl. Phys. Lett.*, 99:121504, 2011.
- [16] Schmitz H. Target normal sheath acceleration sheath fields for arbitrary electron energy distribution. *Phys. Plasmas*, 19:083115, 2012.
- [17] Sherlock M. Universal scaling of the electron distribution function in one-dimensional simulations of relativistic laser-plasma interactions. *Phys. Plasmas*, 16:103101, 2009.
- [18] d’Humières E et al. Optimization of laser-target interaction for proton acceleration. *Phys. Plasmas*, 20:023103, 2013.
- [19] Passoni M, Perego C, Sgattoni A, and Batani D. Advances in target normal sheath acceleration theory. *Phys. Plasmas*, 20(6):060701, 2013.
- [20] Diaw A and Mora P. Thin-foil expansion into a vacuum with a two-temperature electron distribution function. *Phys. Rev. E*, 86:026403, 2012.
- [21] Veltcheva M et al. Brunel-dominated proton acceleration with a few-cycle laser pulse. *Phys. Rev. Lett.*, 108:075004, 2012.
- [22] Sgattoni A, Londrillo P, Macchi A, and Passoni M. Laser ion acceleration using a solid target coupled with a low-density layer. *Phys. Rev. E*, 85:036405, 2012.
- [23] Floquet V et al. Micro-sphere layered targets efficiency in laser driven proton acceleration. submitted for publication, 2013.
- [24] Sgattoni A et al. Enhanced laser coupling and proton acceleration in grating targets by surface wave excitation in the relativistic regime. In *40th EPS Conference on Plasma Physics*, 2013.
- [25] Ceccotti T et al. Evidence of resonant surface wave excitation in the relativistic regime through measurements of proton acceleration from grating targets. submitted for publication.
- [26] Zigler A et al. Enhanced proton acceleration by an ultrashort laser interaction with structured dynamic plasma targets. *Phys. Rev. Lett.*, 110:215004, 2013.
- [27] Gaillard S A et al. Increased laser-accelerated proton energies via direct laser-light-pressure acceleration of electrons in microcone targets. *Phys. Plasmas*, 18:056710, 2011.
- [28] Snavely R A et al. Intense high-energy proton beams from petawatt-laser irradiation of solids. *Phys. Rev. Lett.*, 85:2945–2948, 2000.
- [29] Robson L et al. Scaling of proton acceleration driven by petawatt-laser-plasma interactions. *Nature Phys.*, 3:58–62, 2007.
- [30] Kluge T et al. High proton energies from cone targets: electron acceleration mechanisms. *New J. Phys.*, 14:023038, 2012.
- [31] Zani A, Dellasega D, Russo V, and Passoni M. Ultra-low density carbon foams produced by pulsed laser deposition. *Carbon*, 56:358 – 365, 2013.
- [32] Prencipe I et al. Ultra-intense laser-driven ion acceleration with multi-layered targets. In *40th EPS Conference on Plasma Physics*, 2013.
- [33] Bartal T et al. Focusing of short-pulse high-intensity laser-accelerated proton beams. *Nature Phys.*, 8:139–142, 2012.
- [34] Chen S N et al. Focusing dynamics of high-energy density, laser-driven ion beams. *Phys. Rev. Lett.*, 108:055001, 2012.
- [35] Robinson A P L et al. Spectral modification of laser-accelerated proton beams by self-generated magnetic fields. *New J. Phys.*, 11:083018, 2009.
- [36] Sarri G et al. Dynamics of self-generated, large amplitude magnetic fields following high-intensity laser matter interaction. *Phys. Rev. Lett.*, 109:205002, 2012.
- [37] Macchi A. Toy model of the ”fountain effect” for magnetic field generation in intense laser-solid interactions. *ArXiv e-prints*, 2012. arXiv:1202.0389.
- [38] Fuchs J et al. Tunable achromatic focusing optics for high-current laser-accelerated proton beams. In *1st European Advanced Accelerator Concepts Workshop*, 2013.
- [39] Hegelich B M et al. Laser acceleration of quasi-monoenergetic MeV ion beams. *Nature*, 439:441,



- 2006.
- [40] Schwoerer H et al. Laser-plasma acceleration of quasi-monoenergetic protons from microstructured targets. *Nature*, 439:445, 2006.
  - [41] Levy M C, Wilks S C, and Baring M G. Accelerating piston action and plasma heating in high-energy density laser plasma interactions. *High Energy Density Physics*, 9:198 – 203, 2013.
  - [42] Palmer C A J et al. Monoenergetic proton beams accelerated by a radiation pressure driven shock. *Phys. Rev. Lett.*, 106:014801, 2011.
  - [43] Macchi A and Benedetti C. Ion acceleration by radiation pressure in thin and thick targets. *Nucl. Inst. Meth. Phys. Res. A*, 620:41 – 45, 2010.
  - [44] Robinson A P L. Production of high energy protons with hole-boring radiation pressure acceleration. *Phys. Plasmas*, 18:056701, 2011.
  - [45] Robinson A P L, Trines R M G M, Dover N P, and Najmudin Z. Hole-boring radiation pressure acceleration as a basis for producing high-energy proton bunches. *Plasma Phys. Contr. Fusion*, 54:115001, 2012.
  - [46] Macchi A, Veghini S, and Pegoraro F. “Light Sail” acceleration reexamined. *Phys. Rev. Lett.*, 103:085003, 2009.
  - [47] Macchi A, Veghini S, Liseykina T V, and Pegoraro F. Radiation pressure acceleration of ultrathin foils. *New J. Phys.*, 12:045013, 2010.
  - [48] Q. L. Dong, Z.-M. Sheng, M. Y. Yu, and J. Zhang. Optimization of ion acceleration in the interaction of intense femtosecond laser pulses with ultrathin foils. *Phys. Rev. E*, 68:026408, Aug 2003.
  - [49] Esirkepov T, Yamagiwa M, and Tajima T. Laser ion-acceleration scaling laws seen in multiparametric particle-in-cell simulations. *Phys. Rev. Lett.*, 96:105001, 2006.
  - [50] Aurand B et al. Radiation pressure-assisted acceleration of ions using multi-component foils in high-intensity laser-matter interactions. *New J. Phys.*, 15:033031, 2013.
  - [51] Steinke S et al. Stable laser-ion acceleration in the light sail regime. *Phys. Rev. ST Accel. Beams*, 16:011303, 2013.
  - [52] Dollar F et al. Finite spot effects on radiation pressure acceleration from intense high-contrast laser interactions with thin targets. *Phys. Rev. Lett.*, 108:175005, 2012.
  - [53] Jong Kim I et al. Towards radiation pressure acceleration of protons using linearly polarized ultrashort petawatt laser pulses. *ArXiv e-prints*, 2013. arXiv:1304.0333.
  - [54] Palmer C A J et al. Rayleigh-Taylor instability of an ultrathin foil accelerated by the radiation pressure of an intense laser. *Phys. Rev. Lett.*, 108:225002, 2012.
  - [55] Bulanov S V et al. Unlimited ion acceleration by radiation pressure. *Phys. Rev. Lett.*, 104:135003, 2010.
  - [56] Tamburini M, Liseykina T V, Pegoraro F, and Macchi A. Radiation-pressure-dominant acceleration: Polarization and radiation reaction effects and energy increase in three-dimensional simulations. *Phys. Rev. E*, 85:016407, 2012.
  - [57] Hegelich B M. Towards extreme field physics: Relativistic optics and particle acceleration in the transparent-overdense regime. *Bull. Am. Phys. Soc.*, 56:322 (UI2.00004), 2011.
  - [58] Hegelich B M et al. Experimental demonstration of particle energy, conversion efficiency and spectral shape required for ion-based fast ignition. *Nucl. Fusion*, 51:083011, 2011.
  - [59] Jung D et al. Efficient carbon ion beam generation from laser-driven volume acceleration. *New J. Phys.*, 15:023007, 2013.
  - [60] Haberberger D et al. Collisionless shocks in laser-produced plasma generate monoenergetic high-energy proton beams. *Nature Phys.*, 8:95–99, 2012.
  - [61] Fiuza F et al. Ion acceleration from laser-driven electrostatic shocks. *Phys. Plasmas*, 20:056304, 2013.
  - [62] d’Humières E et al. Investigation of high intensity laser proton acceleration with underdense targets. *J. Phys.: Conf. Ser.*, 244:042023, 2010.
  - [63] Gauthier M et al. Investigation of efficient shock acceleration of ions using high energy lasers

propagating in low density targets. In *39th EPS Conference on Plasma Physics*, volume 36F of *Europhysics Conference Abstracts*, page O2.203, 2012.

- [64] Macchi A, Singh Nindrayog A, and Pegoraro F. Solitary versus shock wave acceleration in laser-plasma interactions. *Phys. Rev. E*, 85:046402, 2012.